Measurement of the Polarization Parameter in K^+p Elastic Scattering*

B. A. Barnett, A. T. Laasanen, P. F. M. Koehler,[†] and P. H. Steinberg

University of Maryland, College Park, Maryland 20742

J. G. Asbury,[‡] J. D. Dowell,[§] D. Hill, H. Kato,[‖] D. Lundquist,[**] T. B. Novey, and A. Yokosawa

Argonne National Laboratory, Argonne, Illinois 60439

G. Burleson[††]

Northwestern University, Evanston, Illinois 60201

D. Eartly and K. Pretzl[‡‡]

National Accelerator Laboratory, Batavia, Illinois 60510

(Received 26 March 1973)

Full angular distributions of the polarization parameter in elastic K^+p scattering at 1.37, 1.45, 1.60, 1.71, 1.80, 1.89, 2.11, and 2.31 GeV/c are presented. These data were obtained in an experiment at the Zero Gradient Synchrotron using a polarized proton target with arrays of scintillation and Čerenkov counters to detect the scattered particles.

I. INTRODUCTION

Precise measurements of the total cross sections for K^+p and K^+d interactions below 3.5 GeV/c have revealed a number of structures in the $I=0$ and $I=1$ channels.[1] The K^+p cross section has a peak at 1.25 GeV/c (see Ref. 2) and several less prominent structures at 1.8 and 2.6 GeV/c.[2,3] If the cross sections in the vicinity of this peak are fitted with the Breit-Wigner resonance formula one obtains the parameters of resonance referred to as the $Z_1(1910)$.[2] Alternatively, these structures could be due to the onset at nearby momenta of the dominant inelastic channels; $K+\Delta(1236)$, $N+K^*(890)$, and $K^*(890)+\Delta(1236)$.[4]

The possibility of resonances in the KN system has aroused considerable interest. The Z_1 with quantum numbers $Y=2$ and $I=1$ could not belong to any of the SU_3 multiplets, $\underline{1}$, $\underline{8}$, or $\underline{10}$, which accommodate all other established hadronic states. At least a 27-multiplet would be required implying the existence of many additional states which have not been seen. Furthermore, in the simple quark model, a Z_1 would be the first example of an exotic baryon, one which cannot be formed from just three quarks.[5] The nonexistence of exotic states is considered essential if the quark model is to retain its appealing simplicity.

Searches for Z resonances with $I=0,1,2$ have been carried out in a variety of production- and formation-type experiments. No experiment to date has produced conclusive results.[6,7,8] A model-dependent analysis of bubble-chamber data on the reaction $K^+p \rightarrow K^0\Delta^{++}$ produces a $P_{3/2}$ partial-wave amplitude which undergoes a counter-clockwise rotation on the Argand diagram. However, the "speed" is inconsistent with a resonance interpretation.[9] Early attempts to find resonances from partial-wave analysis of the elastic K^+p scattering were hampered by lack of polarization data.[10]

The present experiment was carried out to provide the needed polarization data and the results have been reported elsewhere.[11] Full angular distributions of the polarization parameter are reported here for the incident K^+ momenta: 1.37, 1.45, 1.60, 1.71, 1.80, 1.89, 2.11, and 2.31 GeV/c. Similar experiments were done concurrently by groups at CERN and at Yale.[12,13]

The K^+p elastic scattering is also of interest in testing the concepts of duality and exchange degeneracy. Thus, if the Z resonances do not exist, (or are weakly coupled to the elastic channel) then the Regge poles in the crossed channels should be exactly (or approximately) exchange-degenerate. Furthermore, duality would require all Regge amplitudes in K^+p scattering to be real except for the Pomeron which is dual to the nonresonant background.[14] The K^+p system, therefore, provides an opportunity to isolate the Pomeron for use in more stringent tests of duality.[15]

On the basis of these concepts one expects the backward K^+p elastic scattering to be dominated by real exchange-degenerate u-channel trajectories and, aside from small contributions from the Pomeron, one predicts a vanishing polarization parameter.[16] Because of this, special efforts were made in this experiment to obtain precise results for backward scattering at several of the higher momenta.

The main features of the experimental design are

INTERNAL REFLECTION
ČERENKOV COUNTER

POLARIZED HYDROGEN TARGET

DISC

CRYOSTAT

MAGNET

BEAM PATH

A_3, A_4

H_1,$\cdots$,H_6

K^+

BEAM

K^+

A_1, A_2

PROTON A_5, A_6

$C\pi$

S_5

LIQUID Č COUNTERS

θ COUNTERS

BACK-UP COUNTERS
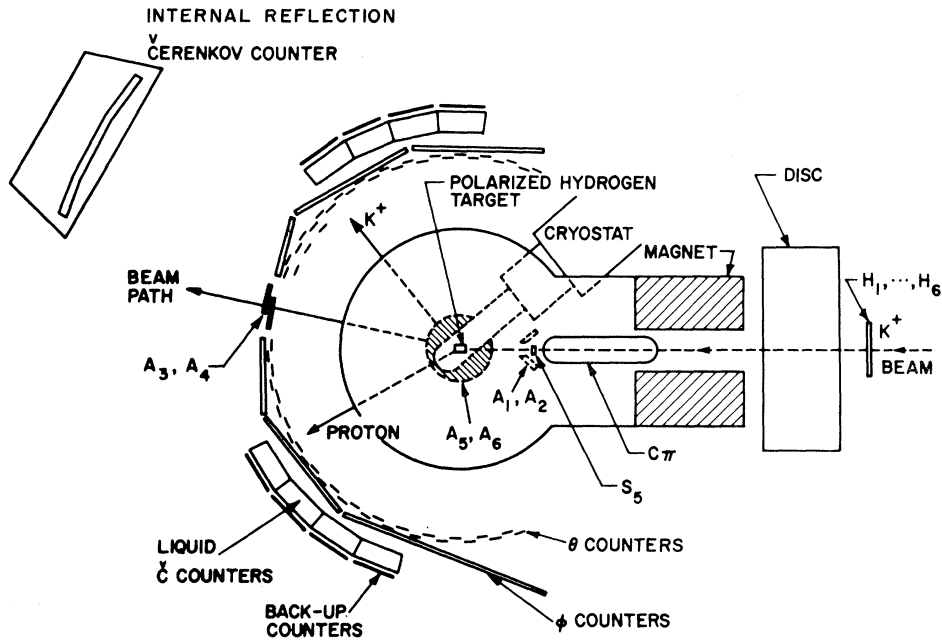
ϕ COUNTERS

FIG. 1. The polarized proton target and the arrangement of counters.

described in Sec. II. Further details of the appara-
tus are given in Sec. III and the methods used in
the data reduction are described in Sec. IV. The
final results are given and discussed in Sec. V.

II. EXPERIMENTAL DESIGN

The arrangement of the counters and target which
are described in this section is shown in Fig. 1.
Kaons were identified by Čerenkov counters in a
partially separated beam of positive particles fo-
cused at the polarized proton target. The free pro-
tons in the small, cryogenically-cooled target
sample were polarized by means of the solid ef-
fect.[17] In this mechanism the direction of the po-
larization, parallel or antiparallel to the fixed
external magnetic field, is determined by the fre-
quency of the continuously-supplied microwave
energy. Three target materials were used. Ini-
tially, a lanthanum magnesium nitrate (LMN) tar-
get was used for measurements at beam momenta
1.37, 1.45, 1.71, and 1.89 GeV/c. The 1.89-GeV/c
measurement was then repeated with a butanol tar-
get and the final stage of the experiment was car-
ried out with an ethylene-glycol target for measure-
ments at 1.60, 1.80, 2.11, and 2.31 GeV/c. Scintil-
lation-counter hodoscopes were placed around the
target on both sides of the beam line. The hodo-
scope counters subtended fixed intervals of either
θ or ϕ in a system of spherical coordinates cen-
tered at the target and with the magnetically-de-
flected unscattered beam as the axis.

The removal of a kaon from the beam was sig-
naled by a veto counter placed downstream of the tar-
get. Whenever a kaon interaction or decay was
accompanied by the detection of particles in both
hodoscopes, the hodoscope data and data from oth-
er selected counters were read into an on-line
computer. Additional veto counters placed above
and below the target reduced the number of events
from inelastic interactions.

The angular correlation between the left- and
right-going particles required by kinematics was
used to select elastic scatterings from the far
more numerous background events. In Fig. 2(a)
this correlation is shown for a beam momentum
of 1.7 GeV/c in which the distortions due to energy
loss and magnetic deflection are included for
events occurring in the center of the target. In
practice, one searches for elastic scattering peaks
in the distribution of θ counter populations, on
the left, say, for particles which are coplanar
with particles in a given θ counter on the right,
or *vice versa*. The single right θ counter will be
referred to as the defining counter and the distribu-
tion of left θ counters is its conjugate distribution.
Any θ counter can be a defining counter. If one
includes the effects of multiple coulomb scattering
and finite target size in smearing the elastic peaks,
it is evident that directional information alone is
not sufficient for distinguishing between the kaon
and the proton in certain angular regions. The
extent of this region of "confusion" can be in-
ferred from Fig. 2(b) where the bands are drawn
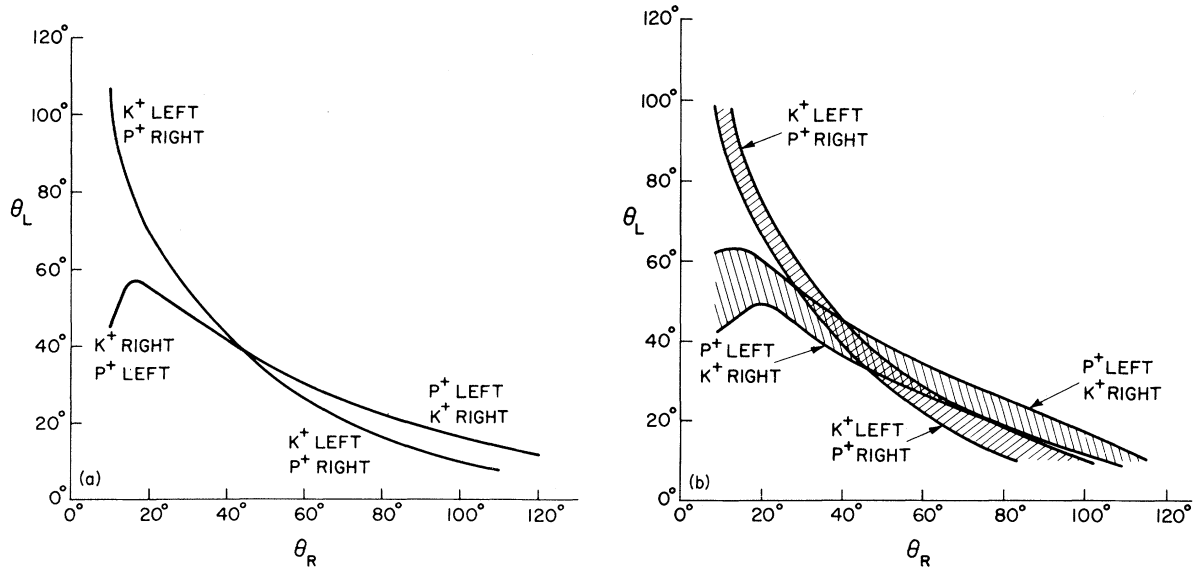
FIG. 2. (a) Relationship between scattering angles in the laboratory for elastic K^+p scattering at 1.7 GeV/c taking into account energy loss in the target and magnetic deflection. (b) The spread in the scattering angles due to multiple-Coulomb scattering and finite target size for elastic K^+p scattering at 1.7 GeV/c.

to include 90% of the events from a Monte Carlo simulation of these effects.

Scattered kaons and recoil protons can be distinguished in these regions by a measurement of velocity. The velocities of elastically scattered kaons and protons as determined at 1.7 GeV/c from the Monte Carlo simulation are shown in Fig. 3.

Liquid threshold Čerenkov counters placed behind the θ counter were used for this purpose. By selecting liquids with suitable refractive indexes, it was possible to cover most of the region of confusion over the range of momenta in the experiment. Data from the Čerenkov counters were read into the computer currently with the hodoscope data.

The polarization direction, which was mainly normal to the plane of scattering, was reversed at frequent intervals and its magnitude was continuously monitored. Populations in the elastic peaks of the conjugate distributions were determined for each polarization setting by subtracting the background, and the polarization parameter was computed from these populations, properly weighted by the average target polarization values and the numbers of incident kaons.

The background subtraction required considerable care since a large fraction of the background was due to quasielastic scatterings with bound protons. These events tended to produce enhancements under the elastic peaks.

Contributions to the background from kaon decays in the τ mode produced additional structures at
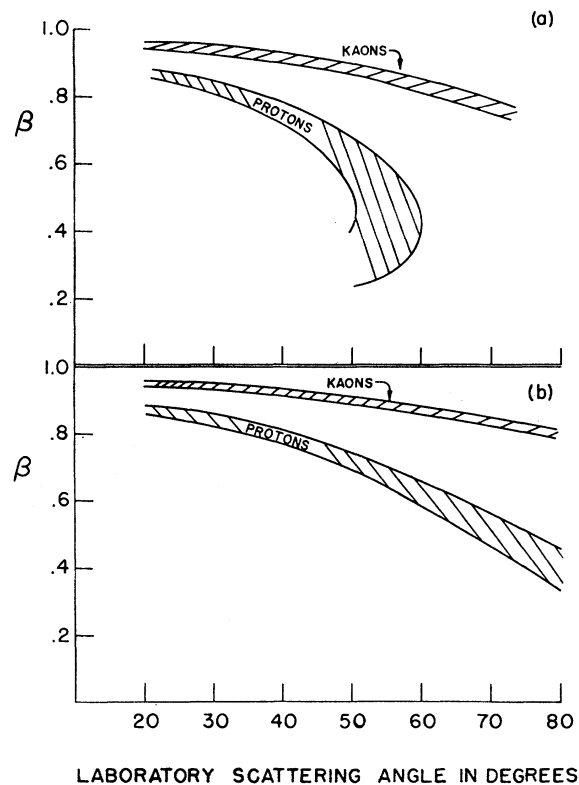
FIG. 3. (a) The distribution of velocities for particles elastically scattered at 1.7 GeV/c into the left hodoscope. (b) The distribution of velocities into the right hodoscope.

forward angles. It was established through com-
parisons with hydrogen-free target runs at 1.37
and 2.11 GeV/c that the background could be deter-
mined by extrapolating the noncoplanar conjugate
distributions under the elastic peaks.

The polarization of the hydrocarbon target was
typically 0.30 to 0.40, whereas the polarization for
LMN was 0.60. In spite of this, the hydrocarbon
targets produced better results because the higher
proportions of hydrogen in these materials resulted
in a substantial improvement in the signal-to-noise
ratio. The effect of this improvement is most im-
portant for backward scattering at higher energies
where the elastic cross sections are very small.
The measurement of the polarization parameter
for backward scattering was further improved in
the final stage of the experiment by introducing an
internal-reflection Čerenkov counter to detect
forward-going protons and on the right-hand side.
Two Lucite threshold Čerenkov counters were in-
stalled in the backward-scattering region on the

left to serve as a veto for pion backgrounds. How-
ever, these counters did not significantly improve
the measurement and were not used in the data
reduction.

III. EXPERIMENTAL DETAILS

A. The Beam and Beam Counters

The arrangement of beam elements is shown in
Fig. 4. A copper target (3 in. long, $\frac{3}{8}$ in. wide, $\frac{1}{8}$ in.
high) located near the upstream edge of the first
bending magnet MB1, was bombarded by 13-GeV/c
protons in an external beam of the Zero Gradient
Synchroton (ZGS) accelerator. Particles produced
at a mean angle of 3° were deflected by BM1 away
from the proton beam line so as to reduce as much
as possible the distance between the first quadru-
pole Q_1 and the production target. The quadrupole
pair Q_1 and Q_2 produced a parallel beam which tra-
versed a fifteen-foot-long electrostatic separator.
In this arrangement the horizontal acceptance of
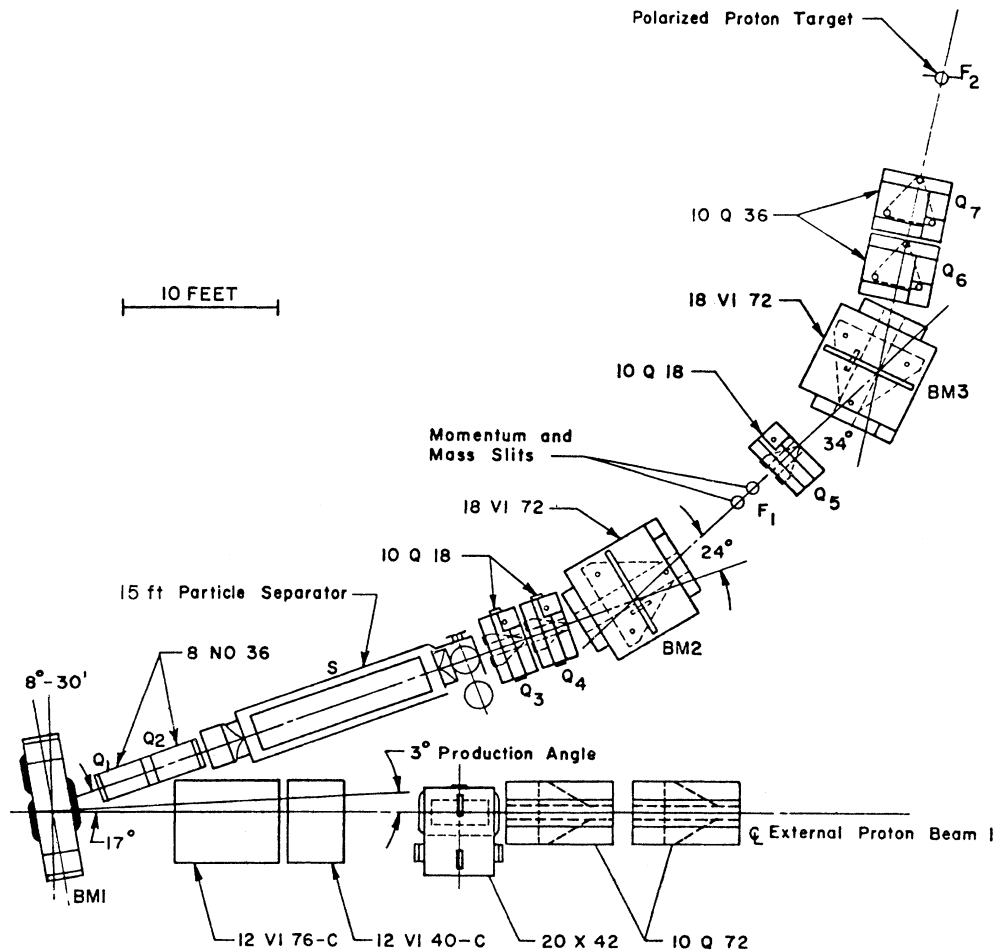
FIG. 4. The layout of the enriched K^+ beam.

± 58 mrad was determined by the aperture of the horizontally focusing Q_1, and the vertical acceptance of ± 7 mrad was determined by the 3.00-inch gap width of the separator. Mass and momentum selection were made at the double focus F_1 and the beam was refocused at F_2 with momentum recombination to a 0.4-in.×0.4-in. spot size. The horizontal and vertical beam convergences at F_2 were $+70$ and ± 6 mrad, respectively and the momentum interval was determined to be $\Delta p/p = \pm 2\%$ for the $\frac{3}{4}$-inch momentum slit opening by a Monte Carlo generation of beam trajectories.

The arrangement of beam counters near F_2 is shown in Fig. 1. The beam was defined by two small counters, S_3 at F_1 and S_5 at F_2, and a six-element hodoscope $H_1, \ldots, H_6$, at the exit of the final quadrupole magnet. Two veto counters A_1 and A_2 flanking the last beam counter were also used to monitor the setting of the final bending magnet BM3.

Kaons were identified in the partially separated beam by a liquid differential DISC Čerenkov counter which also generated an independent pion signal.[18] The DISC signal required an anticoincidence of the passive sum of the nine "pion" phototubes and a 3-fold coincidence of sums of three adjacent "kaon" phototubes. The half angle subtended by the $4\frac{3}{4}$-in. diameter radiating cell near F_2 was 34 mrad, and therefore about one half of the beam kaons were missed.

The efficiency for detecting particles with velocity $\beta \cong 1$ which traversed the $\frac{3}{4}$-inch-thick cell along the axis of the counter was 93 percent. The cell was filled with the liquid C_6F_{12} (FC-51-12). Further discrimination against pions was achieved through the use of a Freon gas threshold Čerenkov counter C_π which was placed close to F_2 in order to minimize the enlargement of the spot size due to multiple Coulomb scattering. The detection efficiency of this counter for pions varied during the course of the experiment but was observed to be as high as 99.95%.[19] Toward the end of the experiment when π^+p and K^+p data were taken concurrently, a second gas counter C_e was introduced inside Q_5 as an electron veto in the pion signal.[20]

The kaon signal B_2 was defined as

$$B_2 = B_1 \cdot H \cdot \text{DISC} \cdot \overline{C_\pi},$$

where

$$B_1 = S_3 \cdot S_5 \cdot (\overline{A_1} + \overline{A_2})$$

and

$H = \sum_{i=1}^{6} H_i$.[21] Background levels in the B_2 signal were less than 0.2% at every momentum except 2.31 GeV/c, where an undiscovered malfunction of the C_π counter resulted in an estimated 10% back-
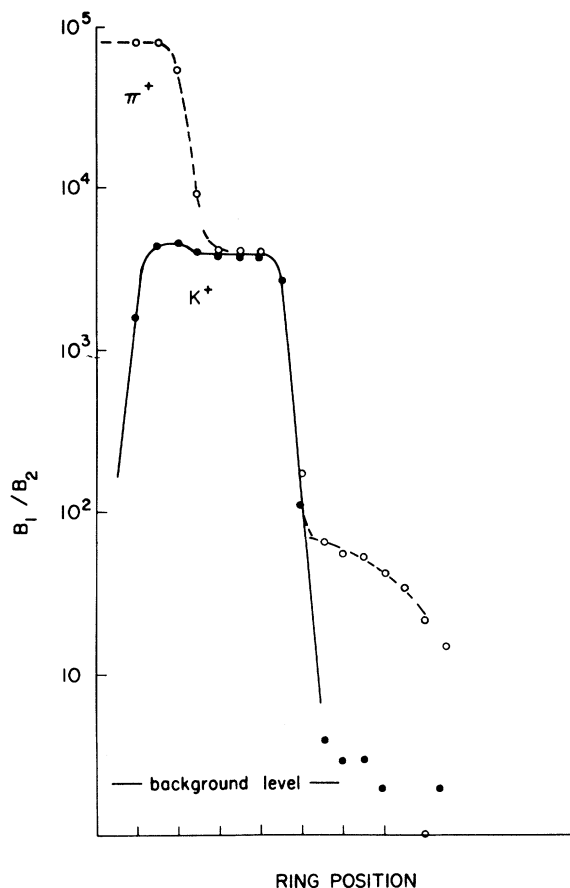
FIG. 5. The response of the DISC counter to varying the Čerenkov angle at 1.74 GeV/c. The solid curve is the standard K^+ signal and the dashed curve is the signal with the C_π veto removed.

ground. The background level was inferred from the variation of B_2 with respect to the position of the phototube assembly which selected the Čerenkov angle in the DISC counter.

In Fig. 5 the plots of the ratio B_2/B_1 are shown for 1.74 GeV/c for the standard kaon signal and for the case where the C_π veto is removed.

The kaon yields at F_2 varied from 4.3×10^3 to 10^4 per 10^{11} protons over the momentum range of the experiment, and the separated ratio of π^+ to K^+ varied from 4 to 40 when the separator was operating at 500 kV. Typical beam proton rates were $(2-2) \times 10^{11}$ per beam spill and the spill time ranged from 700 to 750 msec.

B. Polarized Proton Target

The target used was the ANL Polarized Proton Target—Mark II. The magnetic field was provided by a C-type magnet in which the beam enters

through a 6-inch-diameter hole in the return yoke in order to provide a maximum unobstructed region for the detection of scattering in the median plane. The magnet could provide a highly uniform field of 19 kG for use with LMN, or 25 kG for use with the hydrocarbon targets by selection of appropriate pole shims. The targets were maintained at a temperature of 1° K by horizontal continuous-flow cryostats with diameters which conformed to the two magnet gap widths. The stainless steel and copper walls of the cryostats and the copper target support structures presented to the beam 2.8 g/cm^2 for the LMN, and 2.4 g/cm^2 for the hydrocarbon configurations.

Since the target lengths were 8 g/cm^3 for LMN and 3 g/cm^3 for the hydrocarbons, the contributions to the trigger rates from interactions in the cryostats was substantial. The physical dimensions of the targets were $1\frac{3}{4}$ in. long $\times \frac{3}{4}$ in. for LMN and butanol and 2 in. long $\times \frac{3}{4}$ in. $\times \frac{3}{4}$ in. for ethylene glycol. The LMN target, consisting of La$_2$Mg$_3$ (NO$_3$)$_{12} \cdot$24H$_2$O doped with neodymium, produced polarizations of 0.55 to 0.65. The butanol target, which consisted of frozen butanol with porphyrhexide in packages of FEP plastic, had a polarization which varied from 0.31 to 0.38.

The ethylene glycol (potassium-dichromate oxidized) was contained in tubular FEP packages and the polarization was 0.40 to 0.45.[22] Targets without hydrogen were used to aid in background subtraction. For LMN the dry target was a carefully dried mixture of MgO, CaCo$_3$, C$_5$F$_{12}$ which had nearly the same radiation length as LMN. For the hydrocarbon targets a carbon target was used consisting of baked carbon powder packed into the same type of FEP plastic bags to match the target density.

The polarization was measured at 20- to 30-minute intervals during the experiment, using a nuclear magnetic resonance system in which the NMR signal was proportional to the polarization. The system was calibrated at the small but calculable thermal equilibrium polarization obtained when the microwave power was shut off. This calibration introduced a systematic uncertainty of about ± 0.05 as determined by comparing the asymmetry in *p-p* scattering at 1.34 GeV/*c* with the results obtained by Cheng *et al*. in a double scattering experiment at the same energy.[22]

C. Final-State Detection

1. Hodoscopes

The final-state hodoscope was a system of θ and ϕ scintillation counters on both the left- and right-hand sides of the beam. Each half was firmly supported in a frame which was secured to an aluminum table which could be rotated about a fixed

vertical axis three feet downstream of the target to give easy access to both the target region and the hodoscope itself. The two halves of the hodoscope could also be rotated as a unit about the center of the target magnet. This feature was needed in order to adjust the hodoscope at each momentum so that it was placed symmetrically about the outgoing kaon beam.

The θ-counter hodoscope consisted predominantly of two banks of vertical counters located a nominal 30 in. from the target's center. Alternate counters were staggered forward and backward $\frac{1}{4}$ in. to allow for light tight wrapping on each counter. The angular coverage on each side began at 8° with each counter subtending 3.8° in the median plane. Each had $\frac{1}{4}$ in. thickness, 2 in. width, and a height which was adjusted to give a ϕ coverage of at least ± 14° about the median plane. There were 24 such counters on the right-hand side and 28 on the left-hand side, giving a total angular coverage in the lab of 8° to 104° on the right-hand side and 8° to 120° on the left-hand side.

Three extra θ counters were added to the right half of the hodoscope in the forward direction in order to give a finer $\Delta \cos\theta_c$ definition in that region. These counters, θ_{AA}, θ_{BB}, and θ_{CC}, were placed in front of and overlapping counters $\theta R1$, and $\theta R2$, $\theta R3$ and $\theta R4$, $\theta R5$ and $\theta R6$, and their widths were the same as those of the standard θ counters. Combinations of signals from these counters were used to reduce by one half the width of the θ bins for defining particle directions in that region. The number of defining counters, or θ bins, on the right-hand side was thereby increased to thirty. Consequently, a distinction was made between the θ counters and the θ bins, which were labeled $R1, \ldots, R30$ and $L1, \ldots, L28$.

The ϕ-counter array on each side consisted of seven rows of $\frac{1}{2}$-in.-thick counters, each subtending a constant $\Delta\phi = 3.8°$ as seen from the center of the target. Each of these rows was divided into three sections, the forward two sections being viewed by one phototube and the backward section being viewed by a second tube. This division of the ϕ array maintained a high light-collection efficiency over the entire hodoscope and achieved a particle-detection efficiency of nearly 100%.

2. Liquid Čerenkov Counters

Banks of liquid threshold Čerenkov counters placed behind the hodoscopes on the left- and right-hand sides were used to distinguish between protons and kaons in the region of confusion. Each bank contained four identical counters, each of which covered the angular region of three θ counters. The liquid containers were made of sheet aluminum with dimensions of 3 in. thick, $12\frac{3}{4}$ in.

tall, and $7\frac{1}{2}$ in. at the back. The interior walls
were coated with magnesium-oxide paint to provide
a diffuse reflecting surface with high reflectivity,
and two RCA 8575 photomultiplier tubes were op-
tically coupled to the liquid through short lucite
light pipes at the top and bottom of the counter.

Two methods for calibrating the light sensitivity
of the counter were used to set and maintain a
sensitivity which would yield a high counting ef-
ficiency for kaons and a low efficiency for protons.

The main calibration was provided by an Am^{241}
source encased in scintillation plastic which was
itself encased in lucite for protection. This source
could be inserted into the counter through a stop-
cock-like arrangement in the top without breaking
the light seal. The second calibration was provid-
ed by photodiodes which were attached to the center
of the rear wall of each counter. The photodiode
calibration was continually monitored and signifi-
cant drifts were checked by use of the Am^{241}
source.

The efficiency of the counters as a function of
particle velocity was tested for each of the three
liquids, FC75, water, and glycerol, in a momen-
tum-analyzed positive test beam. A wide range of
particle velocities was achieved by varying the
beam momentum from 600 to 1600 MeV/c and by
using both pions and protons as the triggering
particle. Variations in detection efficiency over
the counter area were not large enough to cause
kaons in one part of the counter to be mistaken for
protons in another part.

The main tests involved finding the detection ef-
ficiencies for different particle velocities at vari-
ous counter-trigger sensitivities, where the sensi-
tivity was defined by the noise-subtracted counting
rate for the Am^{241} source. The data from these
tests gave a family of curves for each of the liquids
relating detection efficiency, particle velocity, and
counter sensitivity. Figure 6 shows the family of
curves for water where the Am^{241} counting rates R
are given in units of 10^3 counts per second.

The important feature of these curves as it re-
lates to the experiment is the fact that for a high
counter sensitivity where the efficiency is nearly
100% just above the Čerenkov velocity threshold,
one finds that the efficiency is as high as 30% just
below this threshold. At a lower counter sensitivi-
ty, where the subthreshold counting efficiency is
small, the efficiency just above threshold is sub-
stantially less than 100%. One observes in the
distributions of velocities in Fig. 3 that the proton
and kaon bands are not widely separated and that
one must deal with a situation where the particles
to be distinguished lie just above and just below
the threshold. Therefore, in order to achieve
clean particle identification the signal from each
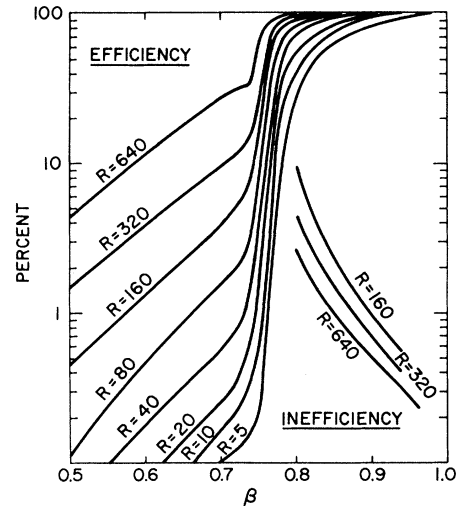
FIG. 6. Efficiencies for the liquid Čerenkov counter
when filled with H_2O for various photomultiplier sensi-
tivities.

counter was fed into two parallel logic systems,
one of which had a high sensitivity for defining
kaons. Any particle which was not detected by the
high sensitivity system was identified as a proton,
and any particle which was detected in the low
sensitivity system was a kaon. Thus, the require-
ment in setting up each counter for taking data was
to select a liquid and two sensitivities which would
best accomplish two things: (1) give the highest
possible particle identification efficiencies, and (2)
keep the level of particle misidentification to less
than about 1.5%. The liquid and sensitivities were
found by combining the velocity distributions from
the Monte Carlo program weighted by the differen-
tial cross section with the counter efficiency
curves like those in Fig. 6. It was always possible
to meet these requirements in all but a small re-
gion of scattering angles where the particle iden-
tification remained ambiguous and the polarization
parameter could not be evaluated.

3. Internal Reflection Čerenkov Counter

In order to improve the polarization parameter
measurements for backward scattering at momenta
1.6, 1.8, 2.1, and 2.31 GeV/c, forward-going protons
were identified by an internal-reflection Čerenkov
counter.

Counters of this type detect particles which pro-
duce Čerenkov radiation which is not trapped by
total internal reflection at the surfaces of the ra-
diating cell. Particles normally incident upon a
flat downstream surface of the cell are detected in
the velocity interval $n^{-1} < \beta < (n^2 - 1)^{-1/2}$ (n is the
refractive index of the cell).

Although this type of counter is usually used for parallel particle beams, it was possible in this case to assure traversal of the cell at normal incidence because a large fraction of the particles originate in the small polarized proton target. The radiating cell was in the form of a spherical shell having a radius of curvature of 66 inches and centered at the target. The counter encompassed particles traversing counters $\theta R1$ through $\theta R4$ corresponding to θ bins $R1$ through $R8$. The index of refraction was so chosen that target protons elastically scattered into this angular range fell within the velocity interval for detection, while the more numerous forward-scattered kaons and pions from inelastic interactions would not be detected.

The cell consisted of two $\frac{1}{8}$-inch-thick circular lucite windows formed into spherical sections of the appropriate radius of curvature and separated by a distance of 1.25 inches. The cell was filled with glycerol and the upstream window was stiffened by styrofoam to provide support against hydrostatic pressure. Eight 58 AVP photomultiplier tubes were mounted around the circular perimeter of the counter and reflecting mirrors were arranged to enhance the illumination of the photocathodes by Čerenkov radiation which was not internally reflected at the downstream window of the cell. A diagram of the counter is shown in Fig. 7. The effectiveness of the counter was limited by a number of factors which gave rise to deviations from normal incidence of the particles upon the

window of the cell. A combination of such effects as the finite target size, multiple coulomb scattering, and variation in magnetic deflection introduced an rms angular deviation of $0.8°$. A calculation based on the kinematics at 1.9 GeV/c showed that for $n = 1.47$ the fastest protons, those traversing $R1$, produced Čerenkov light at an angle which is $1.1°$ less than that required for total internal reflection. On the other hand, the smallest incidence angle of Čerenkov light produced by kaons was $0.8°$ greater than the angle for total reflection. Pions from inelastic interactions were expected to comprise the main background and the Čerenkov angle in this case was $3°$ larger than the reflection angle. Signals from the eight photomultipliers were summed in groups of four by linear mixing circuits and combined to form the proton signal defined as: $F = (\text{top four}) \cdot (\text{bottom four}) + (\text{left four}) \cdot (\text{right four})$.

Requiring an F signal resulted in the reduction of background in the conjugate distributions of $R1, \ldots, R8$ by factors of 2 to 4. Elastic peaks were seen to emerge where they had been totally obscured by the unreduced backgrounds. This effect is seen in the conjugate distribution for $R2$ at 2.11 GeV/c shown in Fig. 8.

FIG. 7. Diagram of the internal-reflection Čerenkov counter.
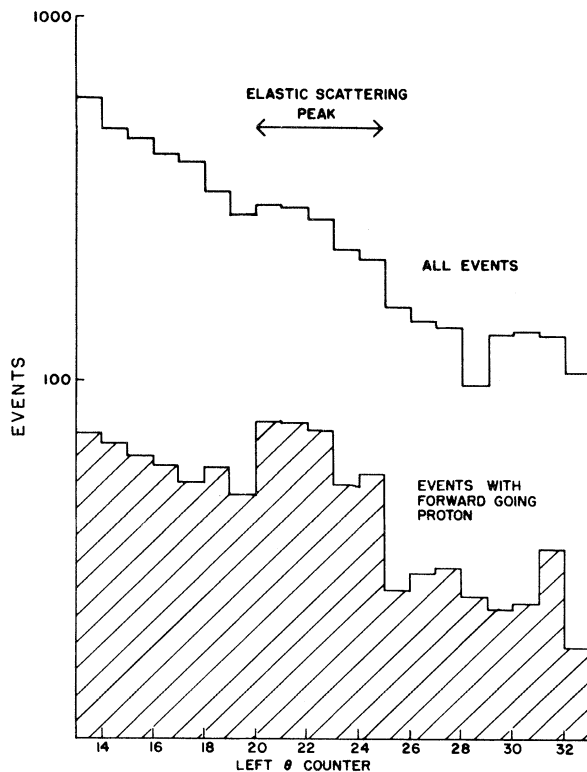
FIG. 8. The conjugate distribution for R_2 at 2.11 GeV/c with and without the internal-reflection counter selection.

D. The Recording of the Data

The fast logic selected likely K^+p elastic scattering events by requiring at least one count in each θ-ϕ hodoscope in coincidence with a disappearing beam kaon. An entering beam kaon was signaled by the coincidence B_2 as described in Sec. II A. The θ-ϕ hodoscope counters were combined into the signals

$$\theta_R = \theta_{R1} + \cdots + \theta_{R24},$$

$$\theta_L = \theta_{L1} + \cdots + \theta_{L28},$$

$$\phi_R = \phi_{R1} + \cdots + \phi_{R7},$$

and

$$\phi_L = \phi_{L1} + \cdots + \phi_{L7},$$

while two downstream beam-veto counters A_3, A_4 and the pole-piece-veto counters A_5, A_6 were combined into the signal $A = A_3 + A_4 + A_5 + A_6$. The event signal or master coincidence (MC) was then defined as

$$\text{MC} = B_2 \cdot (\phi_L \cdot \phi_R) \cdot (\theta_L \cdot \theta_R) \cdot \overline{A}.$$

The liquid Čerenkov counters, the back-up counters, and the internal reflection counter were not required in the fast logic. Coincidences between MC and these signals and signals from the individual θ, ϕ, and beam hodoscope elements were used to set flip-flops for reading into the interface of the on-line computer. The flip-flop data were read and stored in a buffer in the interface which also checked the data for consistency by requiring one, and only one, count in each θ hodoscope before transferring the data to the on-line computer.

The computer used for the experiment was an Advanced Scientific Instrument 6020 with an expanded 16 384 24-bit (plus parity) word memory. The operations of the computer were divided into two parts; data acquisition was carried out during the beam spill, and the data storage and analysis occurred during the proton-acceleration period.

In the analysis the data were checked for consistency (i.e., single counts in each hodoscope) and the events were sorted into arrays according to θ bins L and R and coplanarity $\Delta\phi = |\phi_L - \phi_R|$ in which the ϕ counters were so numbered that $\Delta\phi = 0$ for coplanar events. The θ and $\Delta\phi$ bins were further distinguished where appropriate by data from the liquid Čerenkov counters, the back-up counters, and the internal-reflection counter.

The liquid Čerenkov counters each set two bits, C_H and C_L, from the high- and low-sensitivity signals and the back-up counter set the bit B. A kaon was identified by the requirement $(C_H, C_L, B) = (1,0,1)$ while a proton corresponded to $(0,0,1)$ or, in the event of range limitation, to $(0,0,0)$. The

internal-reflection counter set the bit F so that $F = 1$ indicated a forward proton.

Distributions of the populations in these arrays could be displayed on an oscilloscope during the run for interpretation and equipment monitoring. At the end of each six- to ten-hour run the populations of the arrays were written onto magnetic tape and summed at the end of data taking at each momentum for the asymmetry calculations.

IV. DATA REDUCTION

The asymmetry parameter $P(\theta)$ was computed from the background-subtracted elastic-peak population $N^{\pm}(\theta)$ and the average target polarizations $p_t^{\pm}$ as

$$P(\theta) = \frac{N(\theta)^+ - N(\theta)^-}{p_t^- N(\theta)^+ + p_t^+ N(\theta)^-}.$$

The superscripts $+$ and $-$ correspond to target polarizations being, respectively, parallel or antiparallel with the direction, $\vec{n} = \vec{k}_i \times \vec{k}_f / |\vec{k}_i \times \vec{k}_f|$, where $\vec{k}_i$ and $\vec{k}_f$ are, respectively, the incident and final kaon momentum in the center-of-mass coordinate system. The populations N^+ and N^- were normalized to the total number of beam kaons in each polarization setting and the normalization was also checked by comparison with the numbers of background events in the conjugate distribution. The target polarizations $p_t^{\pm}$ were obtained from the NMR values weighted by the numbers of events transferred to the computer between readings.

The background events which were received along with the desired elastic-scattering events arose from three different sources: (1) kaons scattering from the bound protons in the complex nuclei of the polarized proton target and cryostat walls, (2) kaon decays in flight, and (3) accidentals. The quasifree events produced a broad peak in both $\Delta\theta$ and $\Delta\phi$, centered approximately under the narrow elastic-scattering peak. The width and position of the quasifree peaks agreed with those produced by a Monte Carlo program which randomly chose the initial proton Fermi momentum from the distribution for carbon with the average momentum being 150 MeV/c. These events constituted about 60% of the events when the target was made of LMN and 40% when it was made of alcohol. Kaons which decayed near the target into $K^+ \rightarrow \pi^+\pi^+\pi^-$ produced an enhancement in the forward parts of our conjugate distributions. The total contribution to the data from decays was about 25%. The accidental component of the data was rather small, being about 5% of the total, and produced a generally flat distribution.

The combination of these three sources produced a background which was somewhat structured and which had to be separated from the elastic-scat-

tering events for the polarization calculation. For this reason, data was taken at 1.37 and 2.11 GeV/c using a nonhydrogenous (dry) target which produced no free elastic-scattering events. The data from these runs were compared to the coplanar backgrounds from the regular runs in the regions away from the elastic peak and were found in all cases to be in excellent statistical agreement with no systematic differences.

Given this evidence that the data from the dry target correctly simulated the regular coplanar background, polarization values were calculated using these data as the background under the free elastic peak. At those momenta where we made no dry-target run, we wanted to use the regular noncoplanar distributions normalized in some manner to the coplanar distributions in the region away from the elastic peak as a simulated background under the elastic peak. Many different methods for

making this normalization were examined at 1.37 and 2.11 GeV/c in order to find that method which most consistently produced polarization values in agreement with those produced by the dry target. The normalization method which was selected as best generally ignored the background contributions at θ angles smaller than the elastic peak, and used instead only the region at larger angles. The reason the backgrounds at small θ were not useful was that the main background contribution near the elastic peak came from quasifree events while the forward contribution was mainly from kaon decays. Since these two processes had different coplanarity dependences, with the noncoplanar distributions having relatively more decay and less quasifree contribution than the coplanar cases, it was necessary to avoid the forward region to get a correct background normalization under the free peak. This normalization method produced polarization

TABLE I. Experimental values of the polarization parameters in elastic K^+p scattering as a function of the cosine of the center-of-mass scattering angle θ.

$p_K = 1.37$ GeV/c			$p_K = 1.45$ GeV/c			$p_K = 1.60$ GeV/c			$p_K = 1.71$ GeV/c		
$\cos\theta$	P	ΔP	$\cos\theta$	P	ΔP	$\cos\theta$	P	ΔP	$\cos\theta$	P	ΔP
0.93	0.40	±0.19	0.87	0.53	±0.11	0.91	0.67	±0.16	0.90	0.45	±0.07
0.86	0.43	±0.15	0.78	0.67	±0.06	0.88	0.61	±0.07	0.84	0.64	±0.07
0.83	0.67	±0.22	0.68	0.64	±0.05	0.86	0.63	±0.05	0.80	0.71	±0.09
0.78	0.66	±0.08	0.56	0.65	±0.06	0.81	0.60	±0.05	0.76	0.67	±0.05
0.69	0.63	±0.06	0.50	0.63	±0.10	0.77	0.60	±0.03	0.71	0.71	±0.08
0.58	0.64	±0.06	0.40	0.67	±0.06	0.72	0.56	±0.04	0.66	0.62	±0.04
0.46	0.69	±0.07	0.28	0.70	±0.08	0.68	0.59	±0.03	0.61	0.67	±0.07
0.35	0.76	±0.09	0.21	0.62	±0.06	0.63	0.55	±0.04	0.53	0.67	±0.04
0.23	0.52	±0.08	0.10	0.55	±0.08	0.58	0.56	±0.03	0.40	0.56	±0.06
0.12	0.75	±0.09	−0.01	0.61	±0.08	0.50	0.45	±0.04	0.29	0.48	±0.08
−0.01	0.90	±0.11	−0.13	0.75	±0.09	0.41	0.41	±0.04	0.16	0.58	±0.07
−0.12	0.67	±0.15	−0.24	0.61	±0.12	0.31	0.44	±0.05	0.05	0.49	±0.08
−0.22	0.63	±0.20	−0.33	0.50	±0.15	0.27	0.58	±0.05	−0.05	0.45	±0.12
−0.33	0.59	±0.18	−0.55	0.46	±0.26	0.20	0.46	±0.05	−0.17	0.72	±0.14
−0.43	0.48	±0.23	−0.61	0.23	±0.23	0.16	0.57	±0.06	−0.28	0.09	±0.19
−0.50	0.35	±0.21	−0.67	0.42	±0.36	0.06	0.45	±0.05	−0.36	0.29	±0.46
−0.59	0.61	±0.29	−0.74	0.19	±0.36	−0.03	0.60	±0.08	−0.42	0.30	±0.27
−0.65	0.58	±0.39	−0.79	0.39	±0.59	−0.05	0.52	±0.11	−0.49	0.32	±0.43
−0.71	−0.31	±0.34	−0.84	0.29	±0.32	−0.11	0.40	±0.12	−0.54	0.26	±0.23
−0.76	0.02	±0.36	−0.88	0.44	±0.70	−0.16	0.50	±0.15	−0.60	0.14	±0.36
−0.81	0.23	±0.36	−0.91	−0.12	±0.53	−0.20	0.50	±0.12	−0.66	−0.22	±0.25
−0.85	0.65	±0.89				−0.28	0.53	±0.11	−0.72	−0.34	±0.47
−0.88	−0.46	±0.58				−0.35	0.50	±0.11	−0.83	−0.22	±0.72
−0.91	0.20	±0.89				−0.42	0.37	±0.09			
						−0.47	0.40	±0.21			
						−0.51	0.35	±0.13			
						−0.56	0.43	±0.28			
						−0.62	0.06	±0.16			
						−0.68	0.02	±0.15			
						−0.73	−0.18	±0.15			
						−0.79	0.17	±0.16			
						−0.84	0.37	±0.18			
						−0.88	0.39	±0.25			
						−0.91	−0.07	±0.19			
						−0.96	0.05	±0.25			

TABLE I *(Continued)*

p_K =1.80 GeV/c			p_K =1.89 GeV/c			p_K =2.11 GeV/c			p_K =2.31 GeV/c		
$\cos\theta$	P	ΔP	$\cos\theta$	P	ΔP	$\cos\theta$	P	ΔP	$\cos\theta$	P	ΔP
0.93	0.65	±0.13	0.91	0.52	±0.04	0.95	0.50	±0.23	0.95	0.72	±0.24
0.91	0.57	±0.09	0.87	0.64	±0.06	0.92	0.50	±0.06	0.92	0.72	±0.09
0.87	0.64	±0.05	0.83	0.57	±0.03	0.89	0.49	±0.05	0.89	0.51	±0.08
0.84	0.61	±0.04	0.78	0.55	±0.05	0.86	0.49	±0.04	0.85	0.57	±0.05
0.79	0.49	±0.04	0.74	0.54	±0.03	0.83	0.55	±0.04	0.81	0.50	±0.05
0.75	0.56	±0.03	0.69	0.58	±0.05	0.82	0.36	±0.04	0.76	0.50	±0.07
0.70	0.54	±0.04	0.63	0.53	±0.03	0.77	0.48	±0.04	0.71	0.47	±0.05
0.65	0.55	±0.03	0.59	0.53	±0.05	0.73	0.47	±0.03	0.66	0.43	±0.07
0.56	0.54	±0.03	0.51	0.48	±0.03	0.68	0.43	±0.04	0.59	0.37	±0.06
0.52	0.42	±0.04	0.43	0.40	±0.10	0.62	0.42	±0.03	0.54	0.47	±0.11
0.44	0.44	±0.05	0.38	0.38	±0.06	0.57	0.38	±0.06	0.46	0.33	±0.07
0.41	0.47	±0.04	0.27	0.47	±0.07	0.49	0.35	±0.04	0.32	0.67	±0.16
0.34	0.37	±0.05	0.11	0.72	±0.14	0.35	0.28	±0.07	−0.07	0.16	±0.45
0.23	0.44	±0.05	0.01	0.45	±0.17	0.28	0.33	±0.08	−0.16	0.24	±0.44
0.12	0.41	±0.07	−0.07	0.41	±0.14	0.16	0.29	±0.14	−0.25	0.27	±0.53
0.01	0.35	±0.09	−0.21	0.36	±0.24	−0.03	0.22	±0.19	−0.63	0.46	±0.33
−0.07	0.35	±0.18	−0.37	0.14	±0.20	−0.13	0.17	±0.21	−0.69	−0.10	±0.35
−0.16	0.23	±0.19	−0.48	0.17	±0.45	−0.26	0.24	±0.20	−0.75	0.21	±0.32
−0.21	0.45	±0.21	−0.55	−0.03	±0.24	−0.36	0.06	±0.26			
−0.24	0.18	±0.15	−0.60	−0.01	±0.31	−0.64	−0.15	±0.27			
−0.32	0.43	±0.19	−0.65	−0.29	±0.38	−0.77	0.00	±0.18			
−0.39	0.13	±0.24	−0.71	−0.36	±0.44	−0.89	0.07	±0.17			
−0.45	0.12	±0.26	−0.77	−0.84	±0.61	−0.94	0.56	±0.53			
−0.50	0.25	±0.21	−0.82	0.34	±0.97						
−0.55	0.14	±0.21	−0.86	−0.83	±0.62						
−0.60	0.17	±0.16									
−0.67	0.05	±0.16									
−0.73	0.13	±0.19									
−0.78	0.17	±0.18									
−0.83	−0.11	±0.18									
−0.87	0.16	±0.24									
−0.91	−0.25	±0.22									
−0.96	0.14	±0.25									

results in excellent statistical agreement with those from the dry target and showed no significant systematic differences at either momenta. It was then used with few exceptions as a recipe for calculating polarization results at the other momenta.

The main exception to this method occurred in our very backward data. Here the effects of kaon decay in the background were negligible and statistics were small so that the background on both sides of the free peak was used in the normalization. In all of these cases the elastic peak had to be clearly discernable by eye in agreement with the position predicted by our Monte Carlo program in order to be included in our final results.

After all the polarization values were calculated, certain redundant data were discarded. These arose from the possibility of calculating a polarization value at a given center-of-mass angle by either defining the angle by the kaon on one side and looking at the conjugate proton distribution or by defining the angle by the proton on the opposite side and looking at the conjugate kaon distribution. If polarization values were calculated using kaon selection on one side and then proton selection on the other, the results were obviously not independent. However, they were not totally dependent either, because the elastic peaks covered more than one counter and because our Čerenkov counters were not 100% efficient. Therefore, we discarded data to the extent that we always took the kaon as the angle-defining particle in such cases and only accepted proton-defining data when the corresponding kaon data could not be used. This occurred mainly where the kaon passed through a liquid Čerenkov counter which could not make a clean particle selection, or when the kaon was very backward scattered and the conjugate proton passed through the forward internal-reflection counter.

This still left two independent sets of data at each momentum, except at 1.89 GeV/c where, because of the use of two different targets, there were four sets. Statistical comparisons between the sets of

data were made and always showed good agree-
ment. Therefore, they have been statistically
combined where there was angular overlap.

V. RESULTS AND DISCUSSION

Values for the polarization parameter along with
their statistical errors for the eight incident mo-
menta are given in Table I. The data for incident
momenta, 1.37, 1.45, 1.71, and 2.10 GeV/c are
shown in Fig. 9, along with the data from the
CERN[12] and Yale[13] groups. The over-all agree-
ment is good and any discrepancies are within the
± 5 per cent normalization uncertainty present in
each of the experiments. The polarization is char-
acterized by a rapid rise from zero at $t = 0$ to a
large positive value ranging from 0.5 to 0.8 depend-
ing upon the momentum. At the higher momenta
$P(\theta)$ falls off to a small value at the backward
angles. The best data for backward scattering are
at 1.80 GeV/c and these are shown in Fig. 10. The
average polarization for $-u \leqslant 0.32$ (GeV/c)^2 is

+ 0.03 ± 0.08 and is consistent with zero. This
result is in agreement with the prediction of a
vanishing polarization parameter for exchange-
degenerate baryon Regge amplitudes, as would
be required by duality if the Z resonance does not
exist.

These data along with data for total cross sec-
tions and elastic differential cross sections have
been used in a large number of partial wave analy-
ses of the K^+p system.[13,23-31] These analyses dif-
fer significantly from each other in a number of
ways. Some analyses are energy-dependent,[26,27]
while the others are energy-independent with some
form of shortest- or smoothest-path selection be-
tween solutions at different energies. The various
analyses also differ in the manner in which the
higher partial waves are treated. Some of the
analyses determine the higher partial waves from
Regge pole models.[24,28,30,31] The others truncate
the angular-momentum distribution at some maxi-
mum l quantum number beyond which no further
improvement of the χ^2 for the fits are obtained.
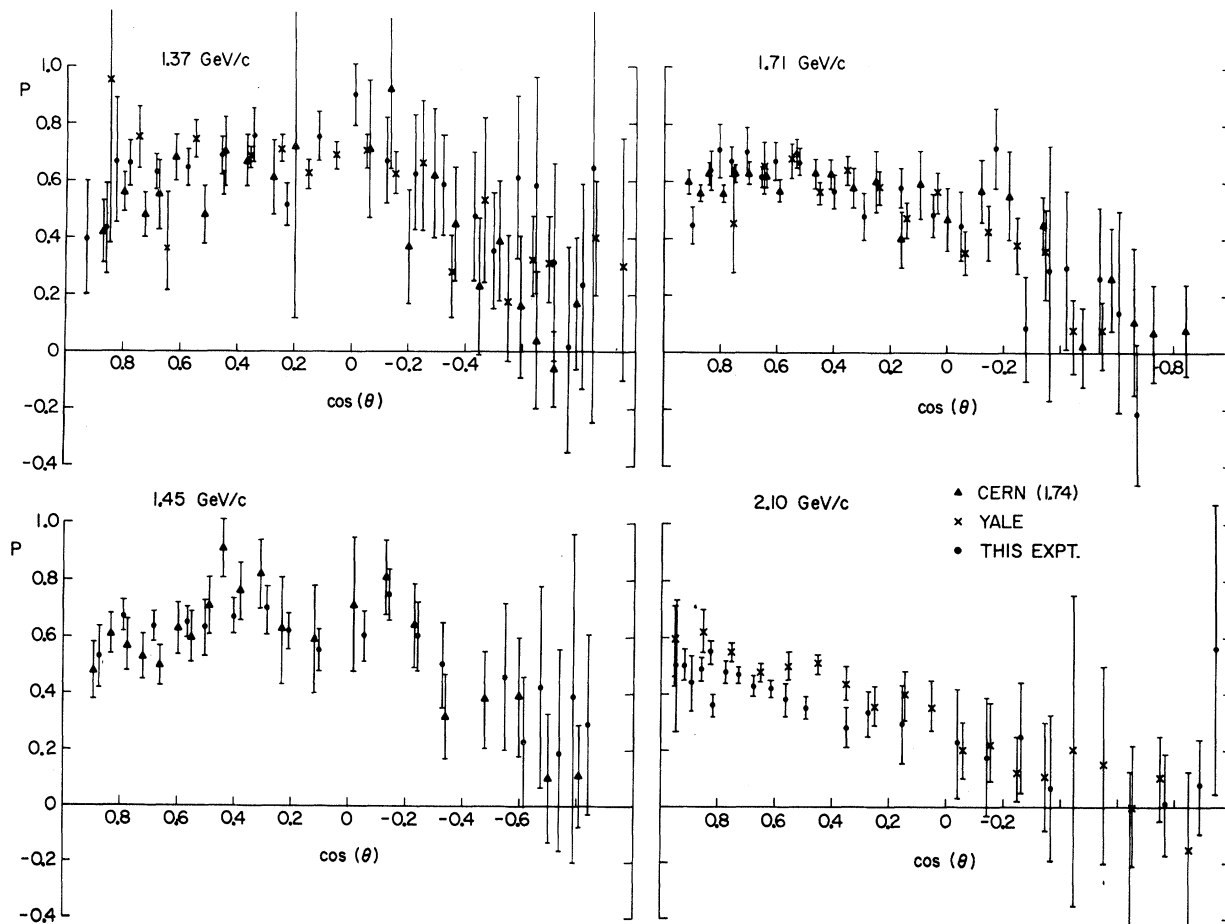
FIG. 9. The polarization parameter at 1.37, 1.45, 1.71, and 2.10 GeV/c in comparison with data from Refs. 12 and 13.
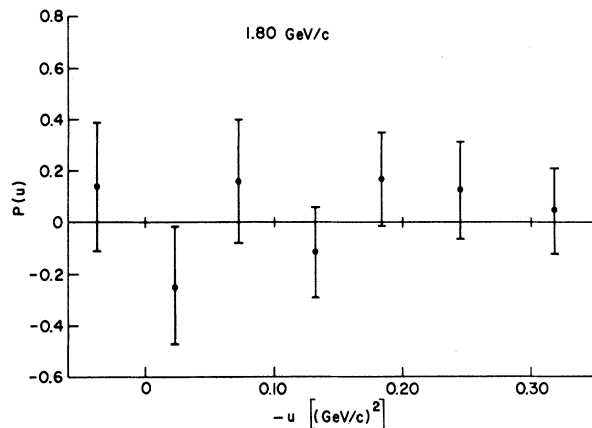
FIG. 10. The polarization parameter at 1.80 GeV/c in the region of the scattering angle in the center-of-mass; $-1.0 < \cos\theta < -0.67$.

There are also differences in the range of energy encompassed in the analysis with the maximum extending to 2.5 GeV/c incident momentum.[13,29,31]

In spite of these differences the results are qualitatively similar. Of special interest is the $P_{3/2}$ partial-wave amplitude which exhibits a counter-clockwise trajectory $T(E)$ on the Argand diagram. Such behavior is characteristic of a Breit-Wigner resonance amplitude. The interpretation of the effect as being due to a resonance is hampered by the presence of a sizable nonresonant background which in some analyses is itself

changing rapidly with energy.[29] The speed defined as $|dT/dE|$ should have an energy dependence which is described by the Breit-Wigner resonance formula. However, the errors in the partial wave amplitudes derived from the currently available data are too large and any resonance behavior in the speed tends to be obscured. Although only a few analyses claim a Z^* the others do not rule out the possibility of its existence. One must conclude from this that the present status of the Z^* from elastic K^+p scattering is inconclusive.

ACKNOWLEDGMENTS

*Work supported by the U. S. Atomic Energy Commission.

†Now at Argonne National Laboratory, Argonne, Illinois.

‡Present address: 1755 E. 55th St., Chicago, Illinois 60615.

§Visitor at the Argonne National Laboratory from the University of Birmingham, Birmingham, England.

‖Present address: Institute for Nuclear Study, University of Tokyo, Tomashi, Tokyo, Japan.

**Present address: Bryant Computer Products, 850 Ladd Road, Walled Lake, Michigan 48088.

††Present address: Department of Physics, New Mexico State University, Las Cruces, New Mexico 88001.

‡‡Present address: Max Planck Institute for Physics, Munich, West Germany.

[1]Gerald Lynch, *Hyperon Resonances—70*, edited by E. C. Fowler (Moore, Durham, N. C., 1970).

[2]R. L. Cool, G. Giacomelli, T. F. Kycia, B. A. Leontić, K. K. Li, A. Lundby, and J. Teiger, Phys. Rev. Lett. 17, 102 (1966).

[3]R. J. Abrams, R. L. Cool, G. Giacomelli, T. F. Kycia, B. A. Leontić, K. K. Li, and D. N. Michael, Phys. Rev. Lett. 19, 259 (1967).

[4]R. W. Bland, M. G. Bowler, J. L. Brown, J. A. Kadyk, G. Goldhaber, S. Goldhaber, V. H. Seeger, and G. H. Trilling, Nucl. Phys. B13, 595 (1969).

[5]M. Gell-Mann, Phys. Lett. 8, 214 (1964); O. W. Greenberg, *Proceedings of the Fifth International Conference on Elementary Particles, Lund, 1969*, edited by G. von Dardel (Berlingska Boktryckeriet, Lund, Sweden, 1970), p. 403.

[6]V. W. Hughes, *Hyperon Resonances—70*, edited by E. C. Fowler (see Ref. 1), p. 349.

[7]E. W. Anderson, E.J. Blesser, H. R. Bleiden, G. B. Collins, D. Garelick, J. Menes, F. Turkot, D. Birnbaum, R. M. Edelstein, N. C. Hein, T. J. McMahon, J. Mucci, and J. Russ, Phys. Lett. 29B, 136 (1969).

[8]G. Bassampierre, Y. Goldschmidt-Clermont, A. Grant, V. P. Henri, R. Jennings, B. Jongejans, D. Linglin, F. Muller, J. M. Perreau, R. Sekulin, W. DeBaere, J. Debaisieux, P. Dufour, T. Grard, J. Heughebaert, L. Pape, P. Peeters, F. Verbeure, and R. Windmolders, Phys. Lett. 27B, 468 (1968).

[9]R. W. Bland, M. G. Bowler, J. L. Brown, G. Goldhaber, S. Goldhaber, J. A. Kadyk, V. H. Seeger, and G. H. Trilling, Nucl. Phys. B18, 537 (1970); E. Griffiths, A. Hirata, I. Hughes, D. Jacobs, R. Jennings, B. Wilson, S. Focardi, G. Giacomelli, P. Lugaresi-Serra, F. Rimondi, G. Ciapetti, G. Martellotti, D. Zanello, E. Castelli, and M. Sessa, *ibid*. B38, (1972).

[10]A. J. Lea, B. R. Martin, and G. C. Oades, Phys. Rev.

165, 165 (1968).

[11] J. G. Asbury, J. D. Dowell, S. Kato, D. Lundquist, T. B. Novey, A. Yokosawa, B. Barnett, P. F. M. Koehler, and P. Steinberg, Phys. Rev. Lett. **23**, 194 (1969); B. A. Barnett, Univ. of Maryland Report No. 70-071, 1970 (unpublished); B. A. Barnett, A. T. Laasanen, P. H. Steinberg, D. Hill, S. Kato, P. F. M. Koehler, T. B. Novey, A. Yokosawa, G. Burleson, D. Eartly, and K. Pretzl, Phys. Lett. **34B**, 655 (1971).

[12] M. G. Albrow, S. Andersson/Almehed, B. Bosnjakovic, C. Duam, F. C. Erne, Y. Kimura, J. P. Lagnaux, J. C. Sens, F. Udo, and F. Wagner, Nucl. Phys. **B30**, 273 (1971).

[13] R. D. Ehrlich, A. Etkin, P. Glodis, V. W. Hughes, K. Kondo, D. C. Lu, S. Mori, R. Patton, G. A. Rebka, Jr., J. E. Rothberg, P. A. Thompson, and M. E. Zeller, Phys. Rev. Lett. **26**, 925 (1971).

[14] H. Harari, Phys. Rev. Lett. **20**, 1395 (1968); P. G. O. Freund, *ibid*. **20**, 235 (1968).

[15] M. Fukugita and T. Inami, Nucl. Phys. **B44**, 490 (1972). UT-140, 1972 (submitted to Nucl. Phys. B).

[16] V. Barger, Phys. Rev. **179**, 1371 (1969).

[17] C. D. Jeffries, *Dynamical Nuclear Orientation* (Wiley, New York, 19xx).

[18] B. A. Leontić and J. Teiger, BNL Report No. 50031 (T-447), (unpublished).

[19] B. A. Barnett, P. F. Koehler, and P. H. Steinberg, Univ. of Maryland Technical Report No. 894 (unpublished).

[20] G. Burleson, D. Hill, S. Kato, P. F. M. Koehler, T. B. Novey, A. Laasanen, and P. H. Steinberg, Phys. Rev. Lett. **26**, 338 (1971).

[21] The conventions used here in the definition of logical operations are as follows: $A \cdot B$ is A and B, $A + B$ is A or B, and $\bar{A}$ is the logical complement of A.

[22] D. Cheng *et al.*, Phys. Rev. **163**, 1470 (1967).

[23] G. A. Rebka, Jr., J. Rothberg, A. Etkin, P. Glodis, J. Greenberg, V. W. Hughes, K. Kondo, D. C. Lu, S. Mori, and P. A. Thompson, Phys. Rev. Lett. **24**, 160 (1970).

[24] S. Kato, P. Koehler, T. Novey, A. Yokosawa, and G. Burleson, Phys. Rev. Lett. **24**, 615 (1970); A. Yokosawa, *Hyperon Resonances—70*, edited by E. C. Fowler(see Ref. 1), p. 367.

[25] B. Barnett, J. Goldman, A. Laasanen, and P. H. Steinberg, *Hyperon Resonances—70*, edited by E. C. Fowler (see Ref. 1), p. 443; Univ. of Maryland Technical Report No. 70-101, 1970 (unpublished).

[26] G. Giacomelli, P. Lugaresi-Serra, G. Mandrioli, F. Griffiths, I. S. Hughes, D. A. Jacobs, R. Jennings, B. C. Wilson, G. Ciapetti, V. Costantini, G. Martellotti, D. Zanello, E. Castelli, and M. Sessa, Nucl. Phys. **B20**, 301 (1970).

[27] P. C. Barber, T. A. Broome, B. G. Duff, F. F. Heymann, D. C. Imrie, G. J. Lush, B. R. Martin, K. M. Potter, D. M. Ritson, L. A. Robbins, R. A. Rosner, S. J. Sharrock, A. D. Smith, R. C. Hanna, A. T. Lea, and E. J. Sacharides, Phys. Lett. **32B**, 214 (1970).

[28] B. Carreras and A. Donnachie, Nucl. Phys. **B23**, 525 (1970).

[29] R. Ayed, P. Bareyre, J. Feltesse, and G. Villet, Phys. Lett. **32B**, 404 (1970).

[30] C. Lovelace and F. Wagner, Nucl. Phys. **B28**, 141 (1971).

[31] R. C. Miller, T. B. Novey, A. Yokosawa, R. C. Cutkosky, H. R. Hicks, R. L. Kelly, C. C. Shih, and G. Burleson, Nucl. Phys. **B37**, 401 (1972).